Molecular Crystals and Liquid Crystals Science and Technology. Section A. Molecular Crystals and Liquid Crystals

Publication details, including instructions for authors and subscription information:
http://www.tandfonline.com/loi/gmcl19

NEXAFS and ARUP Spectroscopy of an Organic Single Crystal: α-Perylene

U. Zimmermann [a], G. Schnitzler [a], V. Wüstenhagen [a], N. Karl [a], R. Dudde [c], E. E. Koch [c] & E. Umbach [a b]

[a] Physikalisches Institut, Universität, Stuttgart, D-70550, Stuttgart, Germany

[b] Experimentelle Physik II, Universität Würzburg, D-97074, Würzburg, Germany

[c] Fritz-Haber-Institut der Max-Planck-Gesellschaft, D-14195, Berlin, Germany

Version of record first published: 24 Sep 2006

To cite this article: U. Zimmermann, G. Schnitzler, V. Wüstenhagen, N. Karl, R. Dudde, E. E. Koch & E. Umbach (2000): NEXAFS and ARUP Spectroscopy of an Organic Single Crystal: α-Perylene, Molecular Crystals and Liquid Crystals Science and Technology. Section A. Molecular Crystals and Liquid Crystals, 339:1, 231-259

To link to this article: http://dx.doi.org/10.1080/10587250008031046

Mol. Cryst. Liq. Cryst., Vol. 339, pp. 231-259
Reprints available directly from the publisher
Photocopying permitted by license only

NEXAFS and ARUP Spectroscopy of an Organic Single Crystal: α-Perylene

U. ZIMMERMANN[a], G. SCHNITZLER[a], V. WÜSTENHAGEN[a], N. KARL[a*], R. DUDDE[c], E.E. KOCH[c] and E. UMBACH[ab]

[a]*Physikalisches Institut, Universität Stuttgart, D-70550 Stuttgart, Germany,* [b]*Experimentelle Physik II, Universität Würzburg, D-97074 Würzburg, Germany, and* [c]*Fritz-Haber-Institut der Max-Planck-Gesellschaft, D-14195 Berlin, Germany*

(Received August 19, 1998; In final form February 24, 1999)

We have studied the applicability of Near Edge X-ray Absorption Fine Structure (NEXAFS) and Angle-Resolved Ultraviolet Photoelectron Spectroscopy (ARUPS) on *insulating organic molecular crystals,* using single crystals of α-perylene as an example. The influences of sample charging were investigated. By employing suitable compensation techniques in combination with partial yield detection, the charging problem could be solved satisfactorily for NEXAFS and partially for ARUPS. The techniques to be described allowed us to obtain NEXAFS spectra with a fairly high energy resolution of $\Delta E = 0.4$ eV. The spectra so obtained for α-perylene *single crystals* display several sharp peaks whose intensities strongly depend on the *polarization angle* of the incident synchrotron radiation. From the angular dependence we derive an average angle of inclination of the molecular planes relative to the (001) cleavage plane of 85°±5° which is in excellent agreement with the angle determined from a full X-ray crystal structure analysis. The various peaks are tentatively assigned to different transitions from C 1s levels to π^* and σ^* final states; some spectral details even reflect influences by the crystal structure. It is noteworthy that useful sample thickness can be anywhere between monolayer and macroscopic dimensions.

1. INTRODUCTION

While the structural and physical properties of a large number of inorganic solids and surfaces have been studied extensively, the great variety of properties that *organic* solids can have or can assume upon suitable treatment (such as e.g. doping) have been attracting broad attention only in the past few years. The recent rapid increase of interest is mainly due to the challenging prospect of a potential usefulness of this huge class of materials. Progress is expected with the development of new active electronic, opto-electronic and electro-optic, all-organic or

* Corresponding author.

organic-on-inorganic ("hybrid") intergrated circuits and other thin film devices for modern information technology and sensing (see e.g. [1–5]). After the first promising application-oriented steps into what has been named "molecular electronics", however, it soon became clear that it was most important to gain a more detailed insight into the basic properties of this class of materials and to uncover their inherent potential for applications. Only with such knowledge it would be possible to microscopically tailor the wanted structures and properties, to get rid of disorder and impurity interferences, and to project device properties and manufactoring techniques. In particular, it appeared important to find answers to such fundamental problems as to the preferential orientation of molecules in vapor-deposited thin films, the possibilities of such systems to grow in epitaxially ordered structures, especially on inorganic substrates, (such as e.g. conventional semiconductor or metal surfaces), and the geometric and electronic properties of organic/inorganic interfaces, e.g. at electrodes. Further, a controlled preparation of well-defined interfaces between highly ordered thin films of two different molecular materials appeared to be an indispensable basis for meaningful physical experiments. Such experiments then should lead to a detailed microscopic understanding, opening up the possibility to optimize the interactions and transport properties and thus develop such systems into useful devices.

As the number of molecules adjacing an interface is rather small (10^{13} – 10^{14}per cm^2, i.e. 10^{-9} – 10^{-10} moles), it is important to apply analytical techniques that are sufficiently surface sensitive. However, most of the available techniques use charged particles; these necessarily cause a certain degree of degradation of the molecular material ("beam damage"), on the one hand, and frequently also lead to perturbations by sample charging, on the other. The latter problem is a rather common one for insulating films with a thickness exceeding a few monolayers ; it turns out to be a particularly serious one if the samples are *macroscopic insulating organic crystals* as studied in this work. There is only little experience available with eliminating charging in organic solids (see e.g. [6–10] and this is not directly transferable to NEXAFS and ARUPS techniques. It appeared necessary therefore to perform basic experiments on possible causes and mechanisms of charging phenomena and on ways of their elimination.

Concerning the choice of suitable organic materials, the requirement of long term physical, chemical and photochemical sample stability in conjunction with promising properties for electronic, optoelectronic, electro-optic or nonlinear optical applications not only calls for substances of sufficiently large molecular weight to display low enough vapor pressure, but also for molecules with structures that are sufficiently complex to bear the potential of exhibiting interesting properties.

Single cystals of perylene were used in the NEXAFS and ARUPS investigations to be presented here, because these were considered to constitute a useful reference system for the interpretation of results obtained with vacuum vapor-deposited thin films of this material, and even of other similar aromatic molecules containing the perylene core. This principal idea will be elaborated in the present paper.

Near edge X-ray absorption fine structure (NEXAFS) and angular-resolved ultraviolet photoelectron spectroscopy (ARUPS) with linearly polarized synchrotron radiation are two well-established surface-sensitive techniques that are especially suitable for detailed investigations of the geometric and electronic properties of adsorbate layers. These methods had already been applied successfully to study some adsorbates of rather complex organic molecules, and even organic crystals with a certain *dark conductivity* (see e.g., [11–31]). To exploit the potential of these methods in its full width and to overcome the charging problems it appeared desirable to try to extend these techniques to *insulating* organic thin films and single crystals. For the present piloting study we chose α-perylene (c.f. fig. 1) as a model system, because this material has a room temperature vapor pressure that is sufficiently low to guarantee a reasonable thin film stability under UHV-conditions, because it is available – for comparison – in the form of rather pure and perfect macroscopic single crystals [32] with a known crystal structure [33], and, last but not least, because it has a favourable molecular arrangement relative to the crystallographic (001) plane (cf. fig. 1) ; this plane can easily be prepared by cleavage. Moreover, the observation of high charge carrier mobilities in zone-refined single crystals [32, 34–36] makes α-perylene attractive as a model substance.

In section 2 we briefly introduce the techniques used; experimental details are given in section 3. In section 4.1 we present and discuss the charging and radiation damage problems and describe ways that successfully led to well-resolved NEXAFS spectra; reasons will be given that explain why useful ARUPS spectra could not be obtained. The NEXAFS data are presented and interpreted in section 4.2. A short conclusion and outlook will follow in section 5.

2. THE NEXAFS AND ARUPS TECHNIQUES

2.1 NEXAFS

In NEXAFS experiments the sample is irradiated with photons from a tunable X-ray source; it is most convenient to use monochromatized, linearly polarized

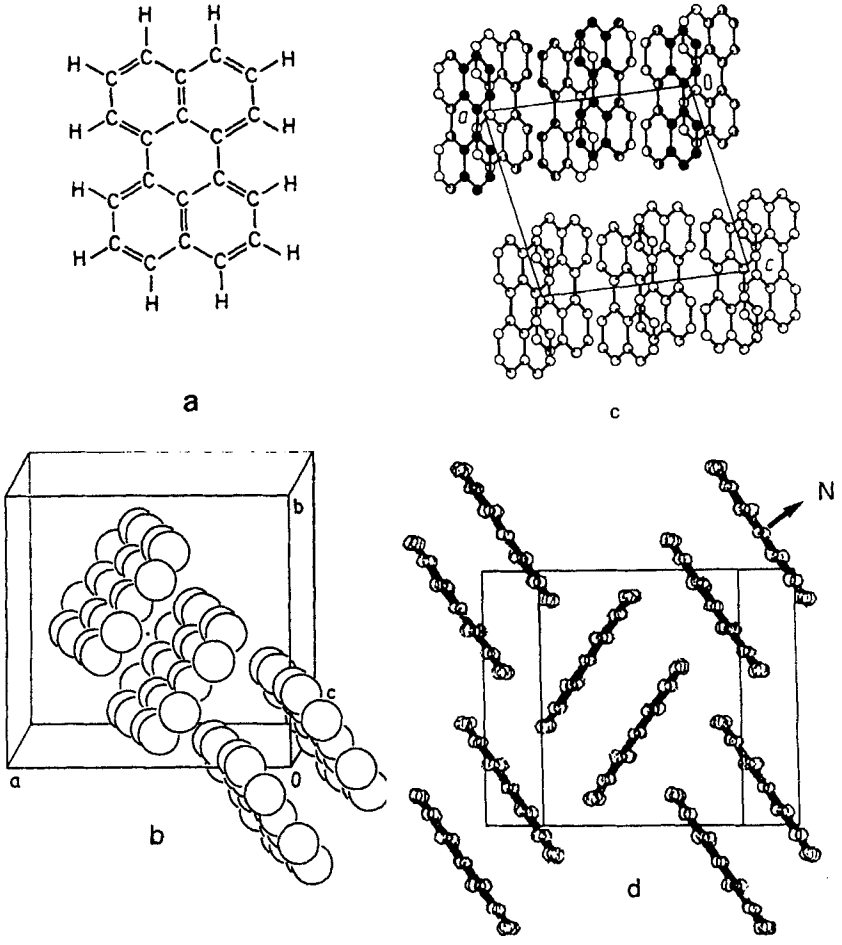

FIGURE 1 The structure of the perylene molecule (a), and the crystal structure of α-perylene in perspective view (b) and in two different, mutually orthogonal projections(c, d): c) projection on the a-c plane (010); the observer views parallel to the a-b (001) cleavage plane, down the 2_1 screw axis [010]; d) projection down the intersection line of the two symmetry-related molecular planes; this line (m) stands under 7° to c′, the normal to the (001) a-b cleavage plane; the cleavage plane is the exposed surface in the experiments; $\sphericalangle(\mathrm{m,a}) = 83°$, $\sphericalangle(\mathrm{m},c') = 7°$, $\sphericalangle(\mathrm{m,b}) = 90°$ .The normals N to the molecular planes make an angle $\gamma = 84.4°$ with c′. – α-Perylene crystallizes in the monoclinic space group $P2_1/a$ with two inversion-symmetric molecular pairs per unit cell. The cell parameters are a = 11.28Å, b = 10.8Å, c = 10.26Å, β = 100.5° (the figure, drawn after the numerical data of ref. [33], has been taken from [36]). Notice that the hydrogen atoms have been omitted in the projections of the unit cell

synchrotron radiation. Absorption spectra are obtained by indirect ("excitation") techniques that monitor a decay signal which is directly related to the absorption

process (e.g. emitted fluorescence photons, Auger electrons, or secondary electrons, emerging from a certain absorption or escape depth), while the photon energy is scanned through an absorption edge. The measured signal is roughly proportional to the absorption coefficient. For an organic molecule X-ray absorption maxima are observed for excitations of a localized 1s core electron (i.e. C 1s, O 1s, N 1s, etc.) to unoccupied molecular states, which can either be bound (i.e. situated below photoionization threshold) or "quasibound" (resonances above threshold that rapidly decay into continuum states).

The NEXAFS transitions, in addition to being element-specific, contain *energetic information* about the chemical binding of the composing elements and molecular groups under consideration and about their interactions. The spectral details are often very sensitive to even subtle differences of the chemical or physical bonding state. Moreover, they contain information about the *spatial* distribution of unoccupied valence orbitals since the transition matrix element involves a very localized 1s initial state. It should be emphasized, however, that this spectroscopy probes valence orbitals in the presence of a core hole, and not those of the unperturbed ground state.

A second important application concerns the *orientation* of molecules. Many organic molecules possess one or more symmetry elements, or at least contain groups that are subject to local symmetry. These symmetry properties can be utilized in polarization-dependent measurements, because the NEXAFS excitations are based on electric dipole transition matrix elements. Consider, e.g., a planar molecule with D_{2h} $(\frac{2}{m}\ \frac{2}{m}\ \frac{2}{m})$ symmetry, such as perylene. The orbitals can be either symmetric "σ"-orbitals with respect to the x-y molecular plane, which is a mirror symmetry plane, or antisymmetric "π"-orbitals. According to the selection rules, only those transitions are allowed whose transition dipole matrix element belongs to the totally symmetric representation (a_{1g}); i.e. the product of the symmetry characters of the three factors of the matrix element – I) the initial state, II) the scalar product of the polarization vector and the dipole operator, and III) the final state – must belong to a_{1g} symmetry. Thus, e.g. for an initial core electron stemming from an s-type level, an excitation into σ-type final state can only take place if the polarization vector also contains σ character (i.e., in the example, if it has a component *in* the molecular plane). In contrast, π-final states can only be reached if the electrical field vector has a component perpendicular to the molecular plane ("π"-component).

If we assume for the moment that *all* molecules (of D_{2h} symmetry, in our example) have the same orientation with respect to a given surface or reference plane of the sample, a *variation of the polarization direction* should, in general, cause a characteristic variation of the height of each of the different absorption

peaks according to the respective symmetry of the final state that is addressed. Consequently, from the variation of absorption with polarization direction and with the knowledge of the σ or π symmetry character of the final state, the orientation of the molecular symmetry element(s) can be concluded. Specifically, for a planar molecule, if the normals of all molecules in an arbitrary sample have the same orientation, a straightforward quantitative evaluation of the *angular variation of the NEXAFS signal intensities* allows one to determine a rather accurate tilt angle γ of the molecular planes relative to the sample surface. The intensity distribution for the $1s \rightarrow \pi^*$ transitions is [37]:

$$I_\pi / I_o \sim P \cdot (\sin\gamma \cdot \cos\vartheta \cdot \cos\varphi + \cos\gamma \cdot \sin\vartheta)^2 + (1 - P)\sin^2\gamma \cdot \sin^2\varphi \quad (1)$$

where I_0 is the intensity of the incident radiation, I the intensity of the NEXAFS signal, $P = I_\perp/(I_\perp + I_\parallel)$ the (generally nonperfect) degree of polarization of the synchrotron radiation, with P = 1 and P = 0 for complete polarization in the plane of incidence and perpendicular to it, respectively. ϑ is the angle of incidence of the radiation relative to the surface normal; the sample rotation angle about the surface normal, φ, is taken as zero when the plane spanned by the molecular normal N and the sample normal is parallel to the plane of incidence.

Usually the molecular arrangement – even in a single crystal – is more complicated. A very common packing pattern of molecular crystals is a zig-zag herringbone-like arrangent of the molecular planes (as in β-perylene) or of pairs of mutually parallel molecular planes, (as realized in the thermodynamically stable modification α-perylene to be used in this work). If such a sample is cut along a plane perpendicular to a crystallographic mirror plane (i.e. along the a-b plane in our case) and oriented such that the mirror plane is parallel to the plane of incidence, then to every molecular normal at azimuth φ a molecular normal at -φ exists. Summing up both contributions the structure of eq. 1 is retained. – If for planar molecules the molecular arrangement relative to the sample surface has at least an (average) threefold rotation symmetry (as e.g. obtained in epitaxy on cubic (111) substrate surfaces) the intensity distribution function of the $1s \rightarrow \pi^*$ transitions is independent of φ

$$I_\pi / I_o \sim P \cdot (\sin^2\gamma \cdot \cos^2\vartheta + 2\cos^2\gamma \cdot \sin^2\vartheta) + (1 - P)\sin^2\gamma \quad (2)$$

If only one of the orientational angles φ and γ of the molecular plane is fixed for all molecules, whereas the other is random, the information that can be obtained is an averaged one; the orientation can be determined less uniquely; moreover, precision suffers in general from a less pronounced (average) anisotropy.

In this paper we have chosen to use only the π^*-intensities for quantitative evaluation, because an analysis of the σ^*-intensities was less save due to ambiguities with peak assignment, very broad peak structures, and unknown background

in the energy range above the absorption edge jump. The results of the angular dependent measurements and of a quantitative evaluation will be presented in section 4.2.

2.2 ARUPS

In angle-resolved UV-photoemission spectroscopy (ARUPS), electronic transitions from occupied molecular orbitals to *continuum* states are monitored. The symmetry character of the latter is determined by the momentum vector of the emitted electrons and hence by the position of the electron analyzer with respect to the reference coordinate system. Since photoemission is also, like NEXAFS, governed by the symmetry characters of the factors in the transition dipole matrix element, the use of polarized synchrotron radiation in conjunction with different angles of incidence can give very similar information. Moreover, cross section effects and band structure formation can be investigated by varying photon energy and angles of incidence and/or detection. Unfortunately in the present case of an *insulating* organic *crystal* charging effects caused very serious distortions and the experimental conditions could not be improved to such an extent that it was possible to obtain sufficiently reliable information from the ARUP spectra; this will be shown and explained below. Therefore the subsequent elaboration will focus on NEXAFS mainly.

3. EXPERIMENTAL

The NEXAFS and ARUPS experiments were performed at the Berlin electron synchrotron storage ring, BESSY [18, 23, 38], using monochromatized radiation from either the SX-700-I [39] or the TGM-1 [40] monochromator. The degree of polarization was $P = 0.87$ for the SX-700-I. In the NEXAFS experiments the monochromator resolution at the carbon K-edge (~ 280 eV) was usually set to 0.7 eV (100 μm exit slit width), in some cases to 0.4 eV (20 μm exit slit) for high resolution measurements. For reasons that will be discussed in section 4.1, the NEXAFS spectra were taken in the partial yield mode; i.e. only those (Auger or secondary) emitted electrons which had sufficient energy to pass a preset threshold potential (established by a retarding electric field) were detected by a channeltron (in the counting mode). The experiments were performed in a UHV chamber, equipped with a hemispherical analyser (VSW), LEED optics, a partial yield detector, and a sample transfer system, described in detail elsewhere [41].

Single crystals of the α-modification of perylene (fig. 1a), studied in these investigations, were grown in the crystal laboratory of the Physikalisches Institut of the University of Stuttgart by the Bridgman technique, using zone-refined material [42]. The crystal structure of the α-modification of perylene has two inversion-symmetrical sandwich pairs of the planar molecule in the unit cell, Z = 4, space group $P2_1/a$ [33], see figs. 1b, 1c and 1d (taken from ref. [36].

Notice that the angle between the c'-axis (⊥ (001)) and the normal N to the molecular plane is 84.4°; i.e. the molecular planes stand nearly upright on the crystallographic (001) cleavage plane (a-b plane) [33], which we have chosen therefore as the surface plane to be studied in the experiments to be presented. The crystal boules were cut into slices along the a-b (001) cleavage plane, using a dissolution thread saw technique; the slices were finally solvent-polished with xylene on lens cleaning cellulose tissue (to a surface roughness of ca. 0.25 μm), see e.g. [42,43].

Two different single crystals of a size of about $5 \times 8 \times 0.6$ mm^3each were used for the measurements to be presented. These samples were placed on a sample holder as shown in fig. 2 and partly covered (and held) by a thin Ni foil, spot-welded onto a Ta support plate which was fixed on grounded stainless steel blocks; electrical contacts to the crystal were made by conductive silver paste. The whole assembly could be transferred across a lock through an evacuated preparation chamber into the measurement vacuum chamber.

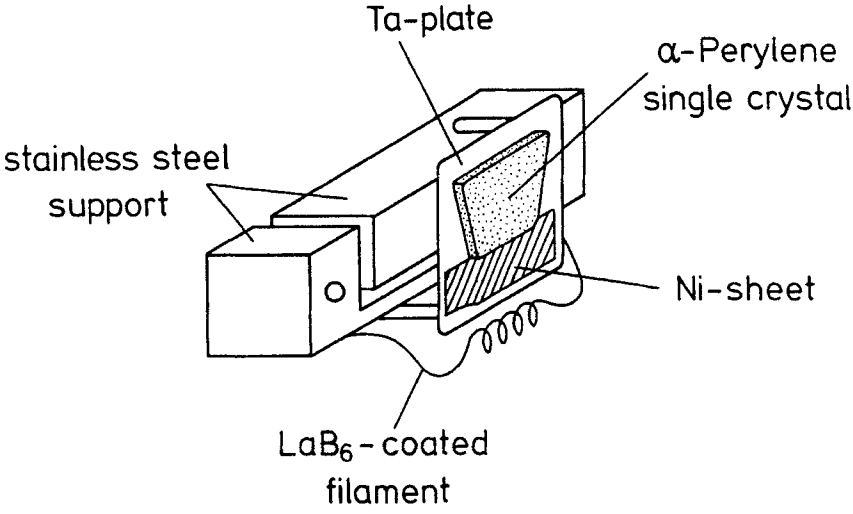

FIGURE 2 Sample holder used in the NEXAFS and ARUPS experiments. For compensation of sample charging a filament was placed near the single crystal, and a Ni-foil, attached to the Ta support plate, was mounted such that it partly covered and contacted the organic crystal

For compensation of positive sample charging a tungsten filament for electron emission was tentatively installed close to the sample (see fig. 2). However, the heat produced with this charge compensation method led to an intolerable increase of the perylene vapor pressure in the chamber. This evaporation was subsequently utilized for cleaning the crystal surface and for sucessively getting rid of radiation damaged molecules from the surface region, but it was, of course, inacceptable for measurements in the synchrotron vacuum system. Therefore we added a LaB_6-coated filament for electron emission at reduced temperature and we cooled the sample holder to about 100 K during the measurements. The perylene partial pressure was thus kept well below 10^{-8} mbar which was considered to be the permissible upper limit.

Intensity normalization of NEXAFS spectra is of prime importance for the evaluation of true peak intensities, in particular at the carbon K-edge [37, 44]. This necessity is due to carbon contaminants on the optical elements of the monochromator which lead to a strongly structured transmission function $I_0(h\nu)$ around the carbon K-edge. In fig. 3 a typical transmission function is shown as dashed line. The signal from the sample, $I(h\nu)$, has to be normalized to the incident intensity I_0 to obtain a true measure of the actual absorption cross section. (An example of a normalized NEXAFS spectrum I/I_0, taken at $\delta = 40°$, is displayed in fig. 3, full line).

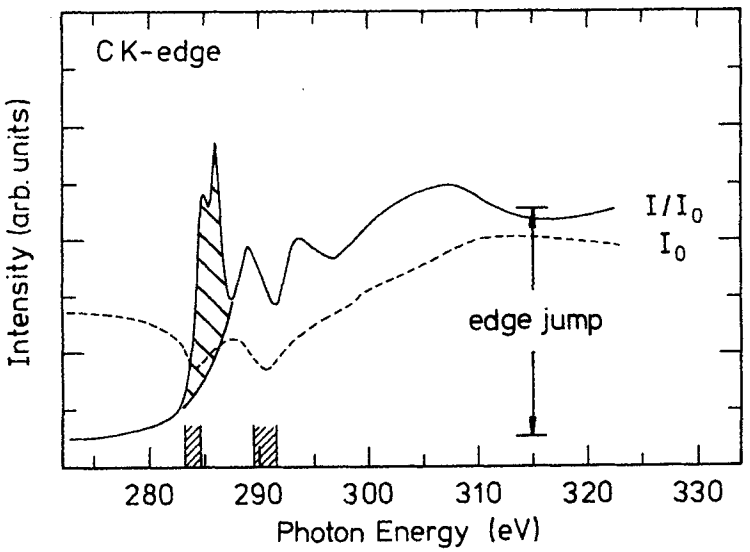

FIGURE 3 Normalized carbon K-edge NEXAFS spectrum I/I_0 of an α-perylene single crystal, taken at an angle of incidence $\vartheta = 40°$ (full line), and the monochromator transmission function $I_0(h\nu)$ used for normalization and energy calibration (dashed line). In the hatched energy regions the normalization procedure is very sensitive to the "correct choice" of the I_0 spectrum. The "edge jump" at the absorption edge as well as the area of the π^* peaks used for quantitative evaluation are indicated

The I_0 signal was recorded by measuring the photocurrent of a gold grid (mesh width 0.5 mm) positioned between the monochromator and the sample. Because the flooding electrons which were needed for charging compensation (see below) strongly contributed to the I_0 signal, a simultaneous recording of I and I_0 was not possible. Normalization was accomplished by recording I_0 with optimized I_0-monitor and I, the partial yield (PY) signal from the sample under optimized charge compensation, in subsequent measurements. In each calculation of the I/I_0 ratio the (slight) decrease of the photon flux caused by the limited lifetime of the electron beam in the synchrotron was taken into account.

The necessary correction of the shape of the spectrum turned out to be considerable (cf. fig. 3, especially in the hatched regions). Therefore extensive investigations were made on the details of the normalization, to make sure that the found peak splitting of the π^*-system as well as the results of the quantitative evaluation given below are correct. In the I_0 signal two dips occurred reprodicibly (cf. fig. 3); these were utilized as references to check the photon energy calibration for each spectrum. The calibration of these apparatively caused dips was achieved by careful XPS measurements (at $h\nu = 300eV$) of samples with accurately known core level energies (Si 2p and Ni 3p), using an energy-calibrated electron analyser. The energies of the two minima so determined were obtained as 284.7 eV and 291.0 eV (±0.1 eV), in agreement with the values reported by Stöhr and Jaeger [37,45].

4 RESULTS AND DISCUSSION

4.1 Handling of charging and radiation damage problems

The study of *nonconductive* organic materials by synchrotron radiation is confronted with several problems. Sample charging, the main problem arising with NEXAFS and ARUPS investigations, will be discussed in subsection 4.1.1. Radiation damage (fragmentation of molecules), a well-known but less restrictive problem which can be solved more easily, is treated in subsection 4.1.2.

4.1.1 Sample charging

Possible effects

Due to insufficient electric dark conductivity of the sample (the band gap of the perylene crystal, ΔE ~3.1 eV [46], is much larger than kT) the photo-, Auger-, and secondary electrons released by synchrotron radiation in the surface region cannot be replaced instantaneously from the bulk. Under the intense irradiation

used (~10^{12} photons mm^{-2} s^{-1}) this leads to the build-up of an inhomogeneous positive surface charge. The additional electric field thus generated in the surface region reduces the kinetic energy of the emitted electrons, and electrons below a certain threshold cannot even leave the sample. Therefore the photoemission peak from a level *i* which should appear at a certain kinetic energy E^i_{kin}, associated with a binding energy E^i_b, is shifted to lower kinetic energy (and thus reflects an apparently higher binding energy). Moreover, because the potential induced by surface charging is not spatially homogeneous, the photoemission peak is broadened asymmetrically. The inhomogeneity arises because the kinetic energy of an electron emitted from an atom B depends on the distance to a previously ionized (and not yet neutralized) neighbouring atom A. Charging shift, peak width, and peak asymmetry are thus a function of the ion – ion separation distribution function that depends on the applied photon flux, the energetic distribution of the emitted secondary electrons, sample size, absorption coefficient and dark conductivity of the material under investigation. Of course, if there is substantial charging, neither ARUPS nor NEXAFS structures can be resolved, as can be seen from fig. 4 for ARUPS and from fig. 5, spectrum 1, for NEXAFS, displayed for demonstration.

Charge compensation techniques

To avoid or at least reduce charging, various techniques were tried; these yielded different success.

1. *Flooding* the sample *with low energy electrons* – a method that turned out to be the most effective charge compensation technique in our investigations. The electrons were emitted either from a

   a) (grounded) filament, located excentrically in front of the sample, and directed onto the latter by a small variable voltage difference (see fig. 2 and section 3), or from

   b) home-made flood gun; the flood gun, however, delivered enough electrons only at kinetic energies above ~8 eV.

(The set-up (a) was applied in the NEXAFS, (b) in the ARUPS measurements). The most drastic effects were always obtained with the flood gun by variation of the magnitude of the compensation electron current (captured by the sample), whereas a variation of the kinetic energy of these electrons had only minor influences on the spectral shape.

2. *Increasing* the sample temperature which should exponentially increase the density of thermally generated charge carriers and hence the dark conductivity, was another method tried.

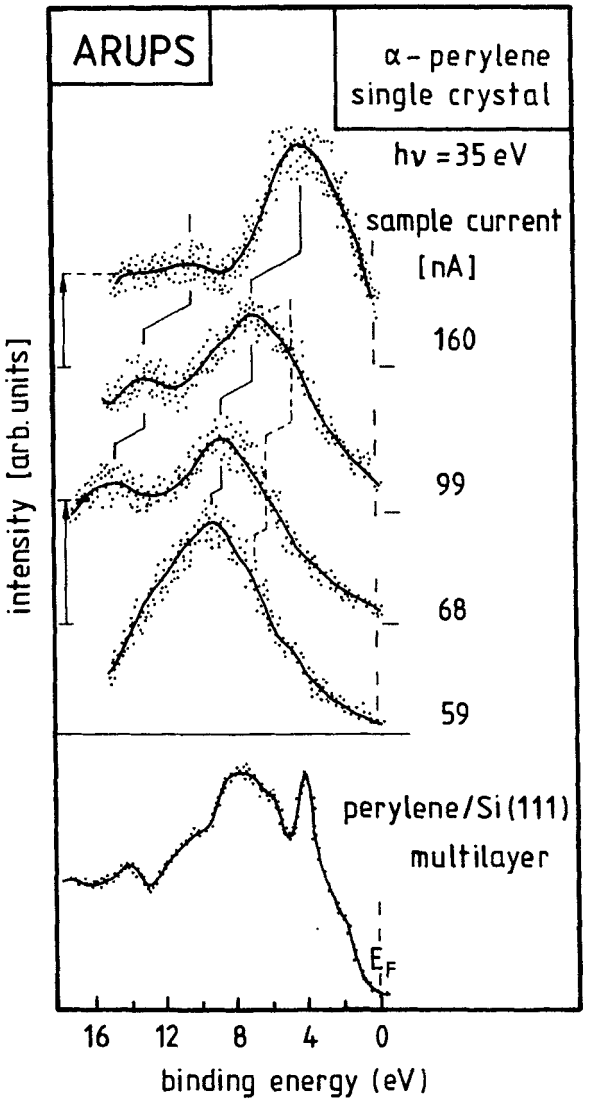

FIGURE 4 ARUP spectra taken at normal emission with hν = 35 eV from an α-perylene single crystal in different states of sample charging, compared to a spectrum of a thin perylene layer (≲ 50Å thick) on Si (111) which displayed no charging effect, cf. [19,47]. The single crystal data were taken at a spot at 5 mm distance from the Ni foil with the HBO lamp shining on the sample. The sample currents caused by the electron flooding are given in the figure. For a suitably selected intermediate value of the current (spectrum 2) the shift is negligible, as desired

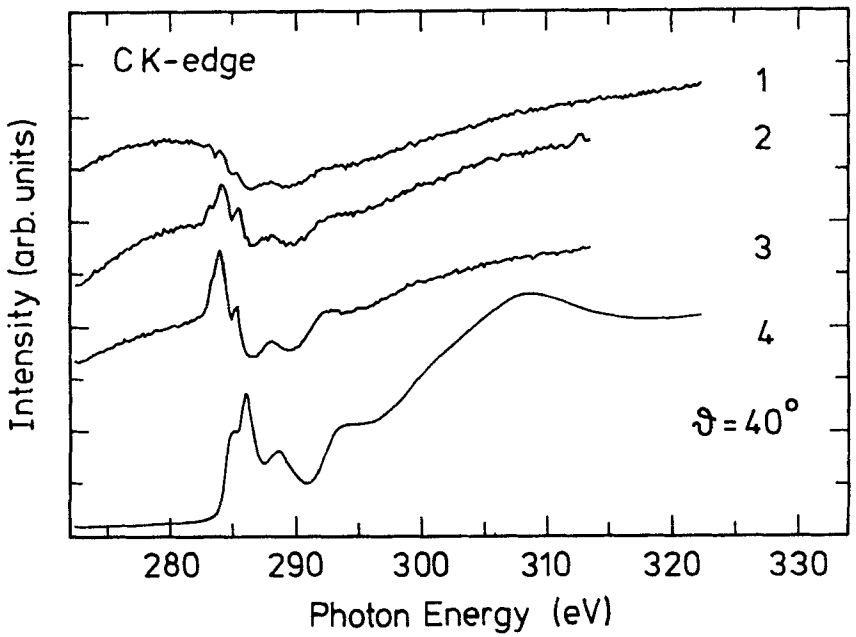

FIGURE 5 Unnormalized carbon K-edge NEXAFS spectra, taken in the partial yield mode of an α-perylene single crystal in different states of sample charging (electron detector signal versus energy of the incident photons). The parameters used for charge compensation while taking the spectra labeled 1 – 4 are given in table I (angle of incidence $\vartheta = 40°$, scan speed 0.4 eV/s, spectral resolution 0.7 eV, retarding voltage for partial yield detection 30 V)

3. *Inducing photoconductivity* by subsidiary illumination in the low energy absorption region with a photon energy too small to cause photoemission (blue/ violet for perylene) is an alternative measure, described in the literature [9]. A high-pressure mercury lamp (Osram, HBO 200), mounted outside the vacuum chamber, was focussed onto the sample for this pupose. Subsidiary irradiation by the Hg lamp generally led to slightly sharper structures. It was therefore left on during all experiments. (Even a normal laboratory tungsten lamp had a noticeable influence.)
4. Improving *charge transport across the crystal surface* by providing subsidiary electrodes at short distances, such as, e.g., a vapor-deposited grounded narrow-mesh metal grid, is an other established possibility to reduce charging, [8, 9], however, with the consequence that emission from the metal is superimposed to some extent. We therefore preferred to try to measure with the synchrotron radiation impinging close to a Ni foil glued off-center onto the crystal surface by conducting silver paint and wired to the sample holder (see fig.2).

Inherent problems with charge compensation

It should be underlined, however, that all efforts made to achieve surface charge neutralisation by electron flooding may lead to overcompensation, i.e. to negative (and usually inhomogeneous) sample charging. This has the consequences of a shift of the photoemission peaks to higher kinetic energy (reflecting an apparently lower binding energy). The *net effect* of simultaneous photoemission and charge compensation by electron flooding can therefore be either no shift, or a slight down or upward shift of the derived binding energy. Even when full net compensation is achieved and hence no net shift of the line centers occurs, the lines will usually be distorted to some extent by (asymmetric) broadening, as discussed above, at least in the case of photoemission (see fig. 4).

4.1.2 Experimental investigations on sample charging

In view of the ambiguity with the proper "a priori" choice of the compensation current,and because of problems with the assessment of an absolute energy scale, inacceptable resolution of spectral details, and poor reproducibility, the spectra obtained in our ARUPS experiments with an insulating organic crystal were considered to be of too little conclusiveness to allow drawing meaningful information. It should not be left be unmentioned, however, that with integral, i.e.non-angular-resolved UPS of perylene and other organic single crystals reasonable data could be obtained successfully under somewhat different experimental conditions (lower photon energies, smaller photon flux, different charge compensation techniques) [7–10].

The recording of useful NEXAFS spectra, however, was rather successful, in contrast to ARUPS. Fig. 5 displays a selection of four NEXAFS spectra taken under the different experimental conditions listed in table I. One can clearly see that spectrum 4 resembles usual NEXAFS spectra, and that the success of charge compensation increased with the number of spectral runs. Spectrum 4 is in fact fully compatible with data from thin perylene layers which are not subjected to charging problems [23]. The origin of the strange shape of spectra 1–3 will be discussed below. We first concentrate on the question how successful the different applied charge compensation techniques actually were for NEXAFS.

TABLE I Experimental conditions for the NEXAFS spectra shown in fig. 5

Curve No.	*filament current (A)*	*distance from Ni-foil (mm)*	*HBO-lamp*
1	0	3	off
2	0	1.25	off
3	0	1	off
4	1.65	2	on

The proximity of the charge collecting Ni foil, mentioned above, had a significant influence on the NEXAFS data, as can be seen from fig. 5. The closer we moved the light spot of the synchrotron irradiation (~ 0.5 mm ∅) to the Ni foil, the more the measured NEXAFS structures became similar to the reference spectrum. This indicates that charge transport across the crystal surface is an important discharge channel, indeed. An enhanced sample temperature obtained by additional heating also reduced charging distortions; but, unfortunately, the concomittant increase of vapor pressure was intolerable in the synchrotron vacuum, as already mentioned.

The most effective charge compensation method was again electron flooding. The success is shown in fig. 5, spectrum 4, and in figs. 3, 7–9. The spectra look quite normal, contain a clear edge jump, and display a fine structure with a resolution which is only limited by the monochromator bandpass. In this case the actual compensation current could not be measured, hence only the current through the filament is given (table I). The average voltage between crystal and filament was a few tenths of a volt and determined by the potential difference between both ends of the filament (the crystal was connected to the positive end of the filament). Note that for filament currents higher than 1.65 A no further changes could be found. The current threshold above which normal NEXAFS spectra were obtained and no further changes occurred, however, depended on sample temperature, proximity of the X-ray spot to the Ni foil, and illumination of the sample by visible/UV light. For the spectra of figs. 3, 7–9 we used the parameters given in the last line of table I.

The conclusion is justified that the NEXAFS method can not only be utilized for spectroscopic investigations of thin films of a great number of *insulating* organic molecular materials, but also of the respective bulk single crystals. *This fact is important because it allows one to use data obtained with bulk samples of known crystal structure and molecular orientation to draw conclusions on the microscopic order and interactions in thin film samples.*

What is the reason for the less favorable behaviour of the ARUPS method as compared to NEXAFS concerning charging interferences?

To find an answer to this question it is necessary to consider the details of the different excitation and detection processes, using the comparison in the schematic fig. 6. The upper part of fig. 6 visualizes the UPS photoemission process from the valence band levels with a binding energy E_b relative to the vacuum-level E_v. By absorption of a UV photon a valence electron is "transferred" towards the right side of the energy scale drawn. Electrons that have energies above vacuum level are emitted with a kinetic energy $E_{kin} = h\nu - E_b$. Thus a spectrum is obtained that has an upper edge (the Fermi level, in case of a metallic conductor, or the top of the uppermost valence band in all other cases) and shows

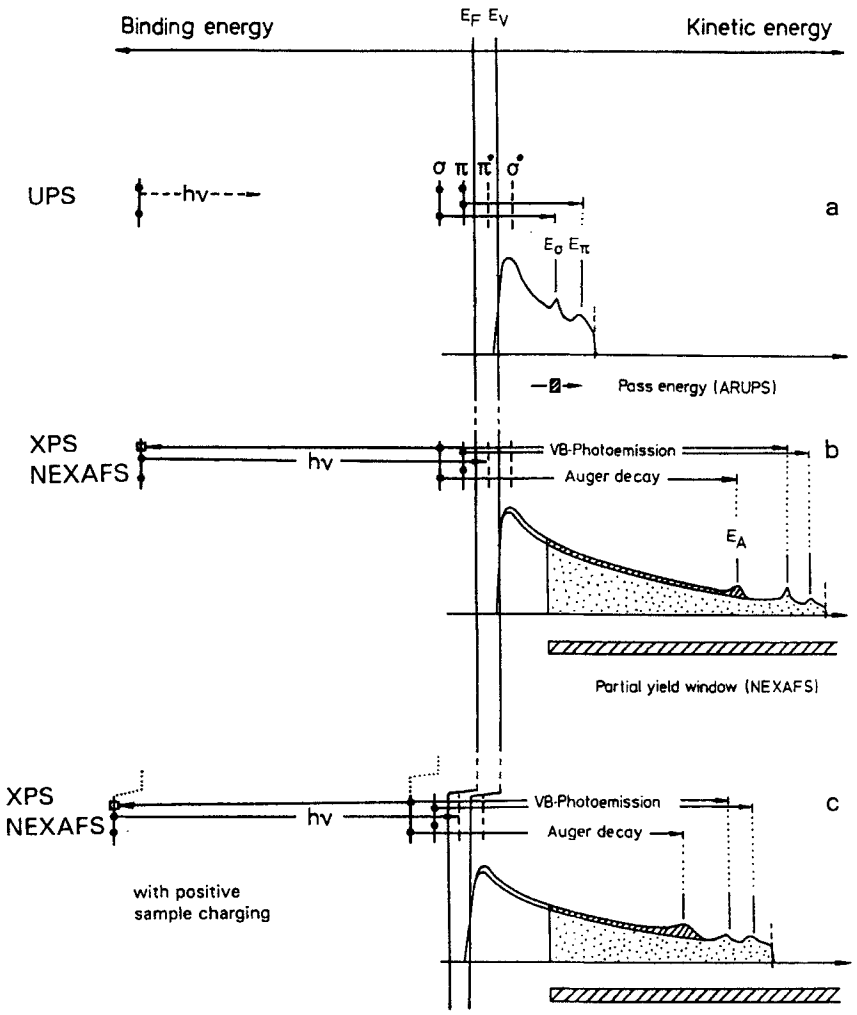

FIGURE 6 Schematic energy level diagram and photoemission spectra for (a) UV-photoemission, (b) X-ray excited photoemission and Auger decay near threshold, and (c): same as (b), but for a positively charged sample. The energy bandpass windows for the detection of photoemission (a) and partial yield NEXAFS (b) and (c) are indicated. Dotted areas represent elastically or inelastically scattered photoelectrons and hatched areas elastically or inelastically scattered Auger electrons recorded by the partial yield detector

peaks which represent occupied valence and core levels. The spectrum also contains a strong background signal caused by secondary (e.g. inelastically scattered) electrons which increases steeply towards low kinetic energy and terminates abruptly at the photoemission threshold (E_v). The spectrum shown

was recorded by scanning an energy window with preset narrow pass width (that determined the resolution) across the kinetic energy range under consideration. If positive (negative) charging had occurred, this spectrum would have been shifted to lower (higher) kinetic energies as discussed above.

In the middle part of fig. 6 a typical X-ray photoemission spectrum (XPS) is sketched. It is rather similar to a UV photoemission (UPS) spectrum, except for the energy range and additional structures. One of such additional structures, an Auger peak, is indicated. The charging problems are similar for XPS and UPS.

However, while for XPS and UPS a fixed photon energy is being used, the photon energy is scanned across an X-ray absorption edge for NEXAFS. This has two consequences for the photoemission spectrum. One is that, as the photon energy is increased, all underlying photoemission peaks continuously shift towards higher kinetic energy. The second effect is the appearance of additional photoemission peaks, whenever the ionization threshold of an occupied electronic level is surpassed, and of Auger peaks at energies E_A in the high energy range of the spectrum which are caused by the decay of the ionized core level, involving two valence electrons in the present case of light elements.

In NEXAFS spectroscopy the X-ray absorption peak positions and peak widths are solely determined by the allowed dipole transitions of the initial (usually neutral) atom or molecule: it is an important feature of NEXAFS that these transitions take place before the emission of a charged particle (the Auger decay is a secondary process) and thus before Coulombic interactions come into play. X-ray absorption energy levels of the neutral atoms or molecules could only be noticeably perturbed by a very high electric field emerging from a charge/ion in the immediate neighbourhood, a situation which is highly unlikely in view of the moderate photon flux density in conjunction with the small cross section for X-ray absorption, as well as in view of the comparatively small "particle" density of eventually accumulated space charge.

The absorption of an X-ray photon in a sample can be monitored by the yield of fluorescence emission (FY), of Auger electrons (AY), or by the total or partial yield of the emission of electrons at different energies (TY and PY, respectively). FY detection was not tried in the present investigation because a suitable X-ray detector was not available. TY detection, easy to perform in principle, caused problems by a poor signal to noise ratio; moreover, small changes of sample charging, causing concomitant shifts of the spectra, drastically altered the TY signal due to the high intensity of secondary electrons near the ionization threshold E_v. Thus TY detection appeared unsuitable for insulating samples.

In what follows, we discuss why *partial electron yield and Auger electron yield detection*of X-ray absorption – that we finally applied – are *less subject to charging distortions* than, e.g., UPS and XPS.

For *Auger yield detection,* AY, a comparatively wide electron pass energy (≥ 10eV) is commonly used for the analyser/detector, with a constant central energy chosen such that the most intense Auger lines fall into this window and are monitored. When the photon energy is scanned across an X-ray absorption edge, an Auger signal is "switched on" (somewhere within the window) with an intensity proportional to the absorption cross section. For samples which charge up, the Auger features are shifted and smeared out, similarly as discussed above for photoemission. But for NEXAFS this is not a serious problem since the pass energy of the analyzer window can be set as large as necessary, such that slight spectral shifts do not matter. What is needed for monitoring the X-ray absorption is merely the integral Auger intensity and not any spectrally resolved structure.

In *partial yield detection,* PY, only electrons in an energy range above a preset retarding voltage (threshold energy E_{th}), indicated in fig. 6 as "partial yield window", are registered, whereas all below are discarded. As the photon energy hν is increased and scanned across an absorption edge at $h\nu_i$, the emission signal above the threshold energy (symbolized by the dotted area in fig. 6) is enhanced by the new Auger peak (processes a and c) and part of the concomitant background of inelastically scattered electrons (indicated by the hatched area in fig. 6). However, a large undesired background signal is suppressed that is caused by the major part of all other inelastically scattered photoelectrons of already opened photoemission channels (e.g. of the transition a) and by the initial low energy part of a freshly opened photoemission channel from the next core level reached: The electrons from these latter contributions appear right above the vacuum level E_v, and their kinetic energy is not enough to surpass the retardation threshold set by the lower limit of the energy window.

Thus one can rationalize that charging influences should even be less significant for the wider window PY than for the narrow window selective AY detection; although this was not explicitely checked in the present investigations, we predominantly used PY detection as it proved to lead to the best S/R ratios in the single crystal experiments and allowed solving the charging problems in a satisfactory way.

There is an additional advantage of PY detection, concerning charging: The choice of the compensation method and of useful parameters is rather uncritical. This is sketched at the bottom of fig. 6. As discussed above, charging leads to a shift of the entire spectrum and to a smearing out of the peaks. Of course, charging occurs already for photon energies below the 1s absorption threshold because of the existence of ionizable levels with lower binding energy (e.g. π valence band states). However, whenever during scanning the photon energy additional absorption channels are opened, there is a strong increase of charging and of the spectral shifts and distortions connected with it. Thus the additional intensity

provided by a newly opened Auger channel may partly or entirely be compensated or even overcompensated by the cutoff of secondary electrons that occurs when – due to charging – the PE spectrum is shifted against the fixed retarding voltage (see fig. 6c). Intensity reduction by overcompensation is clearly seen in the initial NEXAFS spectrum (1) of the series of measurements under successively improved compensation parameters, presented in fig. 5.

Finally we have to answer the question why *charge compensation* works especially well for PY detection. The reason is simply that peak broadening has no effect on the PY signal because this method integrates over the PE and Auger signals. In addition, *small* charging shifts have little influence because the additional intensity gained from a newly "switched on" Auger peak, lying sufficiently above the cutoff threshold energy, and its background is normally much larger than the intensity lost at the lower end of the spectral interval that is accepted by the PY detector.

Summarizing this paragraph we conclude that for the material class of nonconductive organic crystals partial yield (and probably also Auger yield) detected NEXAFS should quite generally be a well-suited experimental method for studies of the electronic and geometric structure if measures against sample charging are taken. The choice of the compensation method and of suitable parameters is rather uncritical. In contrast to NEXAFS, however, ARUPS appears barely useful for such studies even when the charge compensation methods described are applied.

4.1.3 Radiation damage

Radiation damage can be a severe problem for all molecular materials. As a rule, damage is the higher the weaker the chemical bonds and the lower the activation barriers for chemical reactions such as dissociation or formation of new bonds are, and the higher the energy of the photons is. It is often unclear, however, whether the main damage is caused by the primary photoionization process and by a subsequent Auger decay (leading to a *two-hole* final state !), or by the action of the medium energy secondary electrons, for which the ionization cross sections are large. The probability of radiation damage also strongly depends on the rate and degree of delocalization of the locally formed single or doubly charged hole state before bonds have time to change or break by the motion of atoms or molecular subunits.

Since no quantitative predictions are possible, the doses leading to untolerable radiation damage must be checked experimentally in every case. For the present system and the photon fluxes used we observed noticeable irreversible changes in the NEXAFS spectra only after about half an hour.These changes disappeared if the crystal temperature was sufficiently raised such that significant evaporation occurred. Only after hours of irradiation during the alignment procedures of the

experiment visible (brownish) spots with the shape of the illumination focus were seen in the otherwise clear crystal.

Noticeable influences by radiation damage could be avoided by measuring spectra on a fresh sample area in each run (lasting 6 min at most). Thus, in general, with the given diameter of the beam spot d < 0.5 mm, radiation damage should not cause serious problems with organic crystals if reasonably sized samples are available and the molecules have a stability similar to that of perylene.

4.2 High resolution NEXAFS spectra of single-crystalline α-perylene

4.2.1 Assignment of the lower energy peaks

After having solved the experimental problems addressed in the introduction and in section 4.1, reliable NEXAFS spectra of α-perylene single crystal slices could be recorded. Fig. 7 displays a series of normalized spectra taken around the carbon K-edge at various angles of incidence ϑ relative to the crystal surface which is the (001) cleavage plane (see inset). The spectra exhibit a strong angular dependence. For normal incidence ($\vartheta = 0$) the first peaks labeled 1 and 2 exhibit rather high intensity. Increasing the angle of incidence causes a drastic intensity reduction of these peaks whereas the structures labeled 5/6 slightly increase with respect to the edge jump. The (angle-independent) edge jump is defined in fig. 3 and serves as an intensity reference for comparison of the angle-dependent spectra shown in fig. 7.

The spectra of fig. 7 can be used for a first peak assignment (see also table II). Peaks at the low energy onset of a carbon K-edge NEXAFS spectrum of a molecule trivially must be assigned to transitions from the C 1s core level to lowest unoccupied levels. For organic molecules that carry π-electrons these lowest unoccupied levels are antibonding π^*-orbitals. Such π^* orbitals are found in the same energy range for all "unsaturated hydrocarbons" [37; 11–15, 23–28].

TABLE II Assignment of the structurs in the angle-dependent NEXAFS spectra of single crystalline α-perylene in fig. 7

Peak no.	*energy(eV)*	*assignment*
1	284.7(2)	π^*(C=C)
2	286.2(2)	π^*(C=C)
3	289.0(2)	σ^*(C–H), (π^*(C=C))
4	293.6(5)	σ^*(C-C), $\pi \rightarrow \pi^*$shake-up
5	301(1)	σ^*(C-C)
6	309(2)	σ^*, π^*
7	330(3)	σ^*

The intensity of 1s $\rightarrow \pi^*$ transitions should show a strong angular dependence for suitable changes of the molecular orientation. The corresponding experiments, indeed, confirm the assignment of the peaks 1 and 2 of the spectra of fig. 7 to transitions from the 1s core level to π^*-states of the aromatic ring system of the perylene molecule.

4.2.2 Polarization dependence and molecular orientation

The polarization-caused angular dependence of the X-ray absorption can be evaluated quantitatively. In plots of the intensity of the peaks 1 and 2, which were assigned to transitions to π^* final states, as a function of the angle ϑ the dependencies shown in fig. 8 are obtained. When the peak intensities determined as shown in fig. 3 (shaded area) are normalized to the intensity at $\vartheta = 0$, the experimental polarization dependence can be compared with curves calculated for different molecular trial tilt angles γ, using eq. 1. The experimental dependence in fig. 8 is best described by a tilt angle of 85°±5°.

This experimentally determined tilt angle is in excellent agreement with the expected one: The samples used in our experiments had been cut and polished along the a-b cleavage plane which is parallel to (001), (cf. section 3). From the full X-ray crystal structure analysis of α-perylene [19] the inclination angle of the normals of all 4 molecular planes in the unit cell, space group $P2_1/a$, to the normal c′ on the crystallographic (001) plane is obtained as $\gamma = 84.4°$. As the molecular orientations derived from the NEXAFS results obtained with single crystals compare very well with those derived from X-ray diffraction data, we conclude that the NEXAFS method is well-suited not only for the determination of the molecular orientation in single crystals of other aromatic molecules, but also in crystalline thin films and monolayers or even in textured amorphous samples, where X-ray methods are less efficient or even unsuitable. In retrospect, the agreement also gives an unambiguous proof that our assignment of peaks 1 and 2 to transitions into π^* final states was correct indeed.

4.2.3 Fine Structure

For a more detailed analysis of the first peaks fig. 9 displays an expanded scan of the π^* region; spectra taken at two different energy resolutions, $\Delta h\nu = 0.7$eV (100 μm exit slit) and $\Delta h\nu = 0.4$eV (20 μm exit slit) are compared. One can see that the maximum 1 consists of at least two clearly distinquishable peaks with a splitting of ~0.25 eV, and that peak 2 bears a weak shoulder at its high energy tail. The origin of these features and in particular of the large 1.2 eV splitting of peaks 1 and 2 is not fully understood. Recent CNDO/S calculations [47] of the isolated perylene molecule in the ground state yielded only one unoccupied π^*

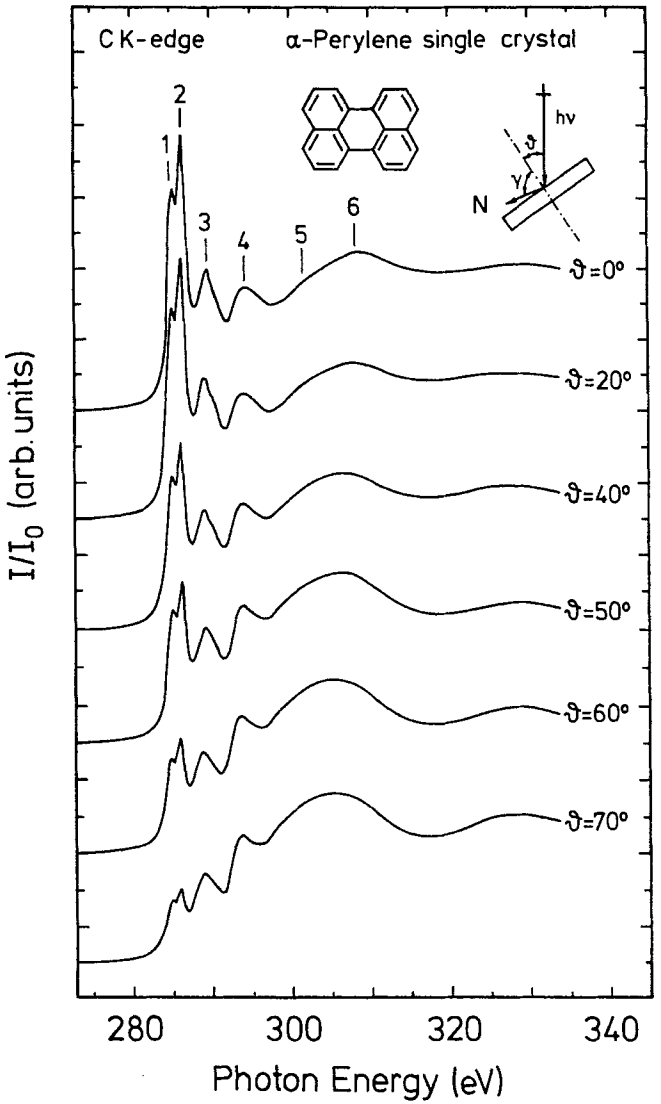

FIGURE 7 Normalized carbon K-edge NEXAFS spectra of a (001)- oriented α-perylene single crystal taken at different angles of incidence ϑ, as indicated. The spectra were recorded in the partial yield mode (energy resolution 0.7 eV, retarding voltage 30 V). The definition of the angles γ and ϑ is shown in the inset. N indicates the average direction of the transition dipole moments of the molecules in the unit cell. The prominent peaks are labeled 1 – 6

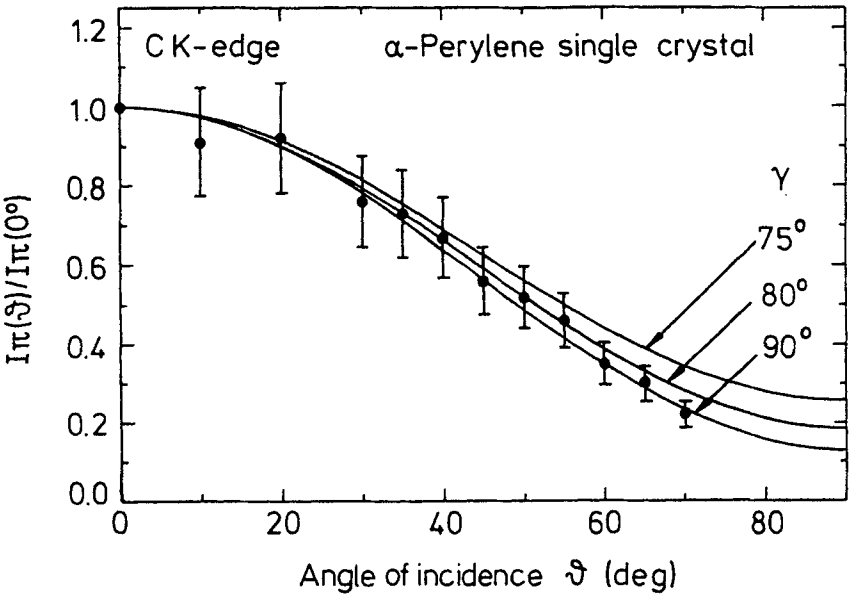

FIGURE 8 Angular dependence of the π^* intensities (hatched area in fig. 3) of the peaks labeled 1 and 2 in fig. 7, normalized to the intensity at $\vartheta = 0$. Dots with error bars represent experimental results; the curves describe the expected angular behaviour – calculated with eq.(1) – for three different inclination angles γ between the average transition dipole moments of the molecules in the unit cell and the surface normal of the sample

orbital in this energy range. However, simple Hückel calculations [23] in "equivalent core" approximation showed that the splitting of peak 1 is most likely due to transitions from C1s levels of inequivalent C atoms into the LUMO, while peak 2 and its shoulders are attributed to transitions into LUMO+1, LUMO+2, LUMO+3 and LUMO+4. Moreover, NEXAFS experiments with *monolayers* and oriented *thin films* published elsewhere [18, 23] gave differing results, in particular fewer peaks and much less splitting in the π^* energy range displayed in fig. 9. For these thin films all molecules were found to lie flat on the substrate surface, thus forming a different structure (with multiple domain orientaions) as compared to the present single crystals. The details of the multiple peak structure and of the differences between single crystals and thin film results are presently under investigation. The splitting is apparently also related to the geometric structure and to the specific interactions between the molecules in the crystalline state. The fine structure of the 1s $\rightarrow \pi^*$ transitions is likely to contain information on details of the organic layers and crystals.

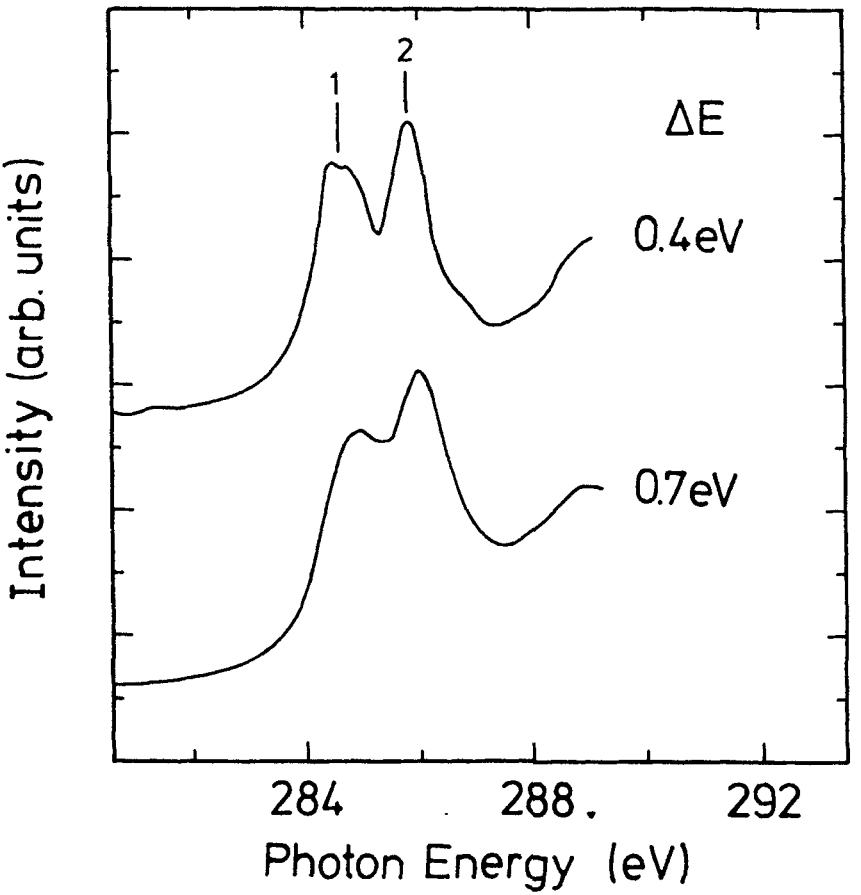

FIGURE 9 High-resolution carbon K-edge NEXAFS spectra of an (001) – oriented α-perylene single crystal surface on an expanded energy scale, with the respective photon energy resolutions ΔE indicated (PY detection mode with 30eV retarding voltage and 1 eV/min scan speed)

A comparison with literature data shows that for a poorly ordered perylene layer on Ag(111) no such splitting in the π^* system has been observed [13], in agreement with our own monolayer and thin film results mentioned above [23]. However, for tetracene and pentacene films on polycrystalline Cu substrates a similar (1 – 1.5 eV) splitting of the π^* peaks, though no fine structure, has been reported [13, 15]. Yokoyama et al. [15] argue that in the case of polyacenes higher unoccupied π^* states have sufficient oscillator strength to be observed in the NEXAFS spectra giving rise to two (or perhaps even more) peaks, whereas in the case of polyphenylenes only one π^* peak was obtained, although these mole-

cules should also have several unoccupied π^* orbitals. This behaviour was explained by these authors by comparisosn with CNDO/S calculations as due to the presence of the core hole. In the case of polyphenylenes this hole leads to a localization of the first π orbital at the core-ionized atom yielding high oscillator strength, whereas the higher π^* orbitals are polarized away from the core hole leading to a considerable decrease of the oscillator strengths. In the case of polyacenes less rearrangement of the surrounding "passive" electrons and hence less localization is expected, which was believed to explain the appearance of a second π^* peak [15]. We partly agree with the localization argument but believe that experiments with higher resolution and more sophisticated calculations are required to arrive at a more detailed understanding of the fine structure.

4.2.4 Assignment of the higher energy peaks

The NEXAFS spectra of fig. 7 display additional peaks labeled 3 – 6. Peak 3 at 289.0 eV is attributed to a $1s \rightarrow \sigma^*$ (C-H) resonance (i.e. to the antibonding final state of the C-H σ-bond). This assignment is based on a comparison with core-excited spectra of cyclic [11, 15, 23, 25–27] as well as linear hydrocarbons [11, 12, 29] and on the sound arguments in refs. [11, 12, 15, 23, 25–27, 29] derived from experimental comparisons and Xα-SW [11, 12, 25–27, 29] or CNDO/S [15] calculations. The fact that this peak shows no polarization dependence (see fig. 7) is consistent with this assignment because the C-H bonds are oriented in all directions in the α-perylene crystal. As no polarization dependence is observable it is not possible to decide whether and to what extent π^*(C=C) final states are superimposed, though such a contribution to peak 3 is likely [12, 48]. However, in contrast to Horsley et al. [48], Yokohama et al. [15] argue that the π^* (C=C) intensity should be relatively small as compared to that of the σ^* (C-H) resonance. Our results support the argumentation of the latter authors.

The intensity of peak 4 at 293.6 eV also appears to be independent of the polarization direction. This would be consistent with its possible assignment to a transition to σ^* (C-C) final states since C-C bonds also occur in all directions in the α-perylene crystal; moreover peaks with similar energies (and σ^* assignment) have been found in other *cyclic* hydrocarbons [12]. Note, however, that the C-C bonds in perylene are not all of the same length. In fact, those C-C bonds which connect the two naphthalene subunits have the longest distance (~1.47Å [33]), these are oriented nearly perpendicularly to the (001) surface (see fig. 2) and hence their σ–transitions should be most intense in the spectra taken at $\vartheta = 70°$, and barely visible in those taken at normal incidence. Although no pronounced such effect is observed here, the measured data can still be considered consistent with the expected polarization dependence since peak 4 exhibits a small peak

shift as a function of the angle ϑ, indicating that it is composed of at least two contributions. The other contribution could represent either transitions to σ^* (C-C) final states of C-C bonds with other bond lengths that are pointing more in directions parallel to the surface, or multiple ("$\pi - \pi^*$shake-up") excitations accompanying the $1s \rightarrow \pi^*$ transitions.

In a similar way the structures labeled 5 and 6 in fig. 7 can be interpreted. Whereas structure 6 hardly shows any angular dependence, the intensity of structure 5 is slightly enhanced for grazing incidence. Features in the energy range above 300 eV can be assigned to higher σ^* resonances which occur predominantly in aromatic systems. The widths (and the small angular dependence of feature 5) are consistent with such an assignment because perylene has many different σ^* orbitals of different symmetry.

The above interpretation in terms of transitions to π^* or σ^* orbitals of local C-C bonds of either more single or more double bond character, however, is questionable, although it follows the common argumentation in literature. In crystalline perylene several different C-C bond lengths exist between 1.37 and 1.48 Å [33] which covers a considerable range between a pure single (1.54Å) and a pure double (1.33Å) bond length. Thus it does not make sense to attribute the observed distinct NEXAFS peaks to transitions of certain local bonds. Rather one should consider the entire system of unoccupied orbitals, their symmetry and energy positions in the presence of core holes, and the corresponding transition probabilities. Since reliable information of this kind can only be expected from detailed calculations which are not yet available, we have tried the conventional assignment here.

5. CONCLUSIONS

In conclusion, we have demonstrated that reliable angle-dependent NEXAFS spectra of an *insulating* organic *single crystal* such as α-perylene can be obtained if sample charging is appropriately compensated. This was achieved by electrons emitted from a hot filament placed near the sample or from an electron floodgun. Further, measures against sample charging basing on an enhancement of the electrical conductivity of the sample (e.g. by thermal and by photoinduced charge carrier generation) were shown to be successful. Moreover, it has been demonstrated that the degree of charge compensation obtainable is sufficient to even allow taking *high-resolution* NEXAFS spectra by the partial yield technique. We were not able, however, to obtain ARUPS spectra with sufficient resolution and reproducibility. For both techniques the charging effects and the influence of the various compensation methods were studied and discussed in some detail. The

different success of NEXAFS as compared to ARUPS measurements can be rationalized as being due to the different type of recording techniques. In contrast to charging, radiation damage and normalization problems could be handled fairly easily.

The NEXAFS structures obtained could be interpreted in some detail. 1s $\rightarrow$ π^*as well as 1s $\rightarrow$ σ^* transitions could be identified unambiguously, whereas the tentative assignment of the peaks above 290 eV has to remain preliminary because sufficiently reliable model calculations are lacking at present. The occurrence of several π^*peaks is plausible, but the strong splitting (> 1 eV) of the two major components is apparently unique for the crystalline state, as it is not found for oriented perylene layers. The strong angular (polarization) dependence of the π^* features could be evaluated quantitatively yielding an average inclination angle of the molecular plane with respect to the surface of 85° ± 5°, in perfect agreement with the results of an X-ray crystal structure analysis.

The results presented indicate that the NEXAFS technique is extremely useful for the investigation of vacuum-deposited (ultra) thin films of big aromatic molecules. For instance, it can be utilized to find the (average) orientation of molecules in textured or microcrystalline layers, or to determine the orientation of epitaxial layers. Moreover, the splitting of the π^* peaks can probably be used to monitor the crystallinity of perylene and other similar thin films. In addition, it may be expected that the comparison of monolayer with single crystal NEXAFS results will lead to a detailed understanding of the geometric and electronic properties of the *interface between organic substances and inorganic substrates.* This is the subject of a separate paper on vacuum-deposited thin films of perylene and perylene-tetracarboxylic-dianhydride (PTCDA) on Si(111) [23].

Acknowledgements

Valuable discussions with J. Taborski are gratefully acknowledged. We are thankful to Chr. Herb for his great engagement in zone refining and crystal growth. This work has been supported by the Bundesministerium für Forschung und Technologie (Projects 05 377 AAB and 477 AAB) and by the Deutsche Forschungsgemeinschaft through SFB 329. The authors E.U. and N.K. would like to thank the Fonds der Chemischen Industrie for financial support.

References

[1] P.M. Borsenberger and D.S. Weiss, *Organic Photoreceptors for Imaging Systems,* (Dekker New York 1993).

[2] G. Horowitz, *Organic Field Effect Transistors,* Advanced Materials **10**, 365 (1998).

[3] D. Wöhrle, L. Kreienhoop, and D. Schlettwein, *Phthalocyanines and Related Macrocycles in Organic Photovoltaic Junctions,* in: *Phthalocyanines, Properties and Applications,* eds.: C.C. Leznoff and A.B.P. Lever, (VCH Publishers, New York 1996) pp. 219–284.

[4] T. Tsutsui and J. Kido eds., *Proceedings of the International Conference on Electroluminescence of Molecular Materials and Related Phenomena, (Fukuoka, Japan 1997),* Synthetic Metals **91**, 3–379 (1997).
[5] J.S. Miller, *Research News/Molecular Materials,* Advanced Materials **2,** 98, 378, 495, 601 (1990); **3,** 110, 262, 564 (1991); 45, 298, **4,** 35, 564 (1992); **5,** 587, 671 (1993).
[6] F.I. Vilesov, A.A. Zagrubski, and D.F. Garbuzov, Fiz. Tverd. Tela **5,** 2000 (1963)
[7] W.D. Grobman and E.E. Koch in: *Photoemission in Solids,* L. Ley and M. Cardona eds., Vol. 2 Chap. 5 (Springer Verlag Heidelberg 1979).
[8] B.M. Schmid, N. Sato, and H. Inokuchi, Chem. Letters 1897 (1983).
[9] N. Sato, H. Inokuchi, B.M. Schmid and N. Karl, J. Chem. Phys. **83,** 5413 (1985).
[10] N. Karl and N. Sato, Mol. Cryst. Liq. Cryst. **218,** 79 (1992).
[11] A.P. Hitchcock, D.C. Newbury, I. Ishii, J. Stöhr, J.A. Horsley, R.D. Redwing, A.L. Johnson, and F. Sette, J. Chem. Phys. 85, 4849,(1986).
[12] J. Stöhr, D.A. Outka, K. Baberschke, D. Arvanitis, and J.A. Horsley, Phys.Rev. B36, 2976 (1987).
[13] P. Yannoulis, R. Dudde, K.-H. Frank, and E.-E. Koch, Surf. Sci. 189/190, 519 (1987).
[14] P. Yannoulis, K.-H. Frank, and E.-E. Koch, Surf. Sci. 241, 325 (1991); Surf. Sci. 243, 58 (1991).
[15] T. Yokoyama, K. Seki, I. Morisada, K. Edamatsu, and T. Ohta, Phys. Scripta, (1989).
[16] K. Seki, N. Ueno, U.O. Karlsson, R. Engelhardt, and E.-E. Koch, Chem. Physics 105, 247 (1986); E.-E. Koch, Physica Scripta T17, 120 (1987).
[17] M.G. Ramsey, D. Steinmüller, and F.P. Netzer, J. Chem. Phys. 92, 6210 (1990); Phys. Rev. 42, 5902 (1990).
[18] U. Zimmermann, G. Schnitzler, N. Karl, E. Umbach, and R. Dudde, Thin Solid Films 175, 85 (1989).
[19] G. Schnitzler, Diplomarbeit, Universität Stuttgart (1989).
[20] E. Umbach, Progr. Surf. Sci. 35, 113 (1991).
[21] D. Schmeißer, A. Jimenez-Gonzales, J. von Schütz, J. Taborski, V. Wüstenhagen, E. Umbach und W. Göpel, Synth. Metals 42, 1809 (1991).
[22] E. Umbach, C. Seidel, J. Taborski, R. Li, and A. Soukopp, Phys. Stat. Sol (b) **192,** 389 (1995).
[23] J. Taborski, P. Väterlein, H. Dietz, U. Zimmermann, and E. Umbach, J. Electron Spectrosc. **75,** 129 (1995).
[24] J. Taborski, V. Wüstenhagen, P. Väterlein, and E. Umbach, Chem. Phys. Letters **239,** 380 (1995).
[25] P. Väterlein, H. Dietz, J. Taborski, W. Wurth, and E. Umbach, J. El. Spectr. Rel. Phen. **78,** 351 (1996).
[26] E. Umbach, R. Fink, M. Jung, P. Väterlein, J. Taborski, and M. Sokolowski, Poverknost. **4/5,** 105 (1997).
[27] E. Umbach, M. Sokolowski, and R. Fink, Appl. Phys. **A 63,** 565 (1996).
[28] D. Gador, C. Buchberger, R. Fink, and E. Umbach, Europhys. Lett. **41,** 231 (1998).
[29] P. Väterlein, R. Fink, E. Umbach, and W. Wurth, J. Chem. Phys **108,** 3313 (1998).
[30] E. Umbach, K. Glöckler, and M. Sokolowski, Surf. Sci., **404,** 20 (1998).
[31] M. Bäßler, R. Fink, C. Buchberger, D. Gador, C. Heske, J. Müller, P. Väterlein, J.U. von Schütz, and E. Umbach, J. Phys. IV, France, **7**, C2–531 (1997).
[32] N. Karl, Mol. Cryst. Liq. Cryst. 171, 157 (1989).
[33] A. Camerman and J. Trotter, Proc. Roy. Soc. London, A279, 129 (1964).
[34] W. Warta, R. Stehle and N. Karl, Appl. Phys. **A36,** 163 (1985).
[35] N. Karl, J. Marktanner, R. Stehle and W. Warta, Synthetic Metals **41–43,** 2473 (1991).
[36] N. Karl in: Landolt Börnstein (New Series) Group III Vol. 17 *Semiconductors,* Subvolume 17i, O. Madelung, M. Schulz and H. Weiss eds., pp. 106–218 (Springer Verlag, Berlin 1985).
[37] J. Stöhr, *NEXAFS Spectroscopy,* (Springer Verlag, Berlin 1992).
[38] U. Zimmermann, Diplomarbeit, Universität Stuttgart (1988).
[39] H. Petersen, Nucl. Instrum. Methods A246, 260 (1986).
[40] W. Gudat, E. Kisker, G.M. Rothberg, and C. Depautex, Nucl. Instrum. Methods A195, 233 (1982).
[41] R. Dudde, Dissertation, Universität Hamburg (1989).

[42] N. Karl in: *Crystals, Growth, Properties and Applications,* H.C. Freyhardt ed., pp. 1–100 (Springer Verlag, Berlin 1980).
[43] R. Stehle, Dissertation, Universität Stuttgart (1984).
[44] D.A. Outka and J. Stöhr, J. Chem. Phys. 88, 3539 (1988).
[45] J. Stöhr and R. Jaeger, Phys. Rev. B26, 4111 (1982).
[46] V.V. Alexandrov, A.I. Belkind, I. Ya. Muzikante, E.A. Silinsh, and L.F. Taure, Sov. Phys. Solid State **18,** 1405 (1976) {Fiz. Tverd. Tela **18**, 2410 (1976)}.
[47] M. Jung, U. Baston, G. Schnitzler, M. Kaiser, J. Papst, T. Porwol, H.J. Freund, and E. Umbach, J. Mol. Structure **293,** 239 (1993).
[48] J.A. Horsley, J. Stöhr, A.P. Hitchcock, D.C. Newsbury, A.L. Johnson, and F. Sette, J. Chem. Phys. 83, 6099 (1985).